45th AIAA Aerospace Sciences Meeting and Exhibit
8 - 11 January 2007, Reno, Nevada

AIAA 2007-557

# A Mesh Deformation Strategy Optimized by the Adjoint Method on Unstructured meshes

Zhi Yang *, Dimitri J. Mavriplis †

*Department of Mechanical Engineering, University of Wyoming, Laramie, WY 82071*

**An adjoint-based optimization procedure is proposed for improving the robustness and extending the range of linear-elasticity-based mesh deformation techniques. Using the values of the modulus of elasticity E defined in each mesh cell as the design variables, the procedure seeks to determine an optimum distribution of E throughout the mesh, in order to minimize a global objective function which reflects the skewness or lack of quality of the deformed mesh. The technique is applied to highly-stretched mixed element meshes in two and three dimensions on complex geometries, and is shown to be capable of recovering a valid mesh in a small number of optimization cycles for cases where the non-optimized linear-elasticity approach fails. However, the solution of the optimization problem remains relatively costly in terms of cpu time, compared to a non-optimized mesh deformation calculation, making this technique best suited for precomputing improved E distributions prior to the simulation, or for use as a plug-in module to be invoked in cases where the non-optimized procedure fails.**

## I. Introduction

Unstructured mesh approaches have become well established for numerical flow simulations due to the flexibility they afford for dealing with complex geometries. For problems involving moving boundaries, such as unsteady aeroelastics, control surface deflection problems, and shape optimization problems, robust mesh deformation techniques are necessary for maintaining a suitable discretization of the evolving computational domain. Several mesh-deformation strategies, such as the tension spring analogy,[2,18] the torsion spring analogy[3,13] and the linear elasticity analogy,[1,14] have been successfully demonstrated in the literature. These methods are designed to produce a valid mesh given a set of prescribed boundary displacements, by recomputing new mesh-point coordinates without the addition/deletion of new mesh points, and without altering the connectivity or topology of the mesh. However, all these methods will eventually fail given large enough boundary displacements, since the original mesh topology cannot be retained indefinitely. On the other hand, resorting to mesh reconnection and refinement/derefinement schemes adds considerable complexity to any numerical simulation procedure, since this generally entails load balancing operations, changing discretization stencils, and introduces non-differentiable procedures into the simulation process, which presents difficulties when linearizations are required, as may be the case for sensitivity analysis within the context of error analysis or shape-optimization problems. Thus, it is important to develop robust mesh deformation strategies which enable the retention of the mesh connectivity for a wide range of problems.

The various mesh deformation methods mentioned above contain a series of model parameters (i.e. spring stiffness, modulus of elasticity) which can be modified to increase the robustness of these schemes. For example, in the context of the linear spring analogy approach, the spring stiffnesses are often taken as inversely proportional to the length of the mesh edge raised to some power p.[18] For the linear elasticity approach, the modulus of elasticity is often taken as inversely proportional to the cell volume.[6,19,20] This formulation of the linear elasticity approach has been found to be particularly robust, since by design, the linear elasticity approach is capable of reproducing solid body motion (translation and rotation) for stiff regions (high modulus of elasticity E). Thus, critical small-cell regions are displaced with little or no relative deformation or strain, and the most severe deformations are relegated to less critical regions of the mesh

*Postdoctoral research associate, AIAA member; email: zyang@uwyo.edu
†Professor, AIAA Associate Fellow; email: mavriplis@uwyo.edu

which can sustain more strain. Alternate prescriptions, such as taking the modulus of elasticity E inversely proportional to the distance from the moving wall have also been found to work well in various cases.[20]

For cases which fail, further robustness improvement can be obtained by modifying the E distribution in regions where poor mesh quality is detected. For example, one approach may consist of prescribing very large values of E at cells which become negative through the deformation process, or alternatively, updating the E values as inversely proportional to the deformed cell volumes while progressively deforming the mesh in a sequence of small steps. One of the drawbacks of this approach is that the mesh deformation equations become non-linear, while the prescription of E as inversely proportional to cell volume remains somewhat arbitrary.

Alternatively, one may ask what is the "best" distribution of E which will result in the highest quality deformed mesh, or which will enable the retention of a valid mesh (positive volume cells) under the largest surface displacements. Once this optimal distribution is determined, the linear mesh deformation problem may be solved to obtain the new deformed mesh. The determination of the best E distribution corresponds to an optimization problem, where the values of E in each mesh cell constitute the design variables, and the objective consists of some description of global mesh quality. Adjoint methods are well suited for these types of optimization problems, which involve a single objective function, and a large number of design variables.[5,11,12,14] In this work, we propose an adjoint-based optimization procedure for determining an optimum or improved E distribution for the linear elasticity mesh deformation approach, which results in a more robust mesh deformation strategy. One advantage of this approach is that it no longer relies on the arbitrary prescription of E as inversely proportional to the cell volume or the distance from the wall. Furthermore, the mesh deformation problem remains linear, and once the optimum E distribution has been determined, the efficiency of the previously developed linear mesh deformation solver is retained. On the other hand, the optimum E distribution is found to depend on the particular prescribed boundary displacement, and, as will be shown, the solution of the optimization problem is generally non-trivial, thus reducing some of the perceived advantages of this approach over the previously mentioned non-linear formulation. However, the resulting E distributions can be expected to result in a more robust mesh deformation process. Furthermore, these optimal E distributions may be precomputed for the most severe mesh deformation cases, and then used subsequently for intermediate steps in the linear mesh motion solution process, thus reducing the overall cost.

In this paper, we formulate an adjoint-based optimization problem for improving the robustness of linear-elasticity mesh deformation techniques, and demonstrate this approach on various complex configurations. In the following section, we first outline the linear-elasticity mesh deformation strategy. We then formulate the optimization problem for improving the robustness of the mesh deformation strategy, including the formulation of the adjoint problem, a suitable objective, and techniques for carrying out the optimization. Solution of the optimization problem can be particularly challenging, given the large number of design variables (three-dimensional set corresponding to millions of mesh cells). Thus, considerable effort must be expended on devising a suitable convex objective function, and using efficient optimization procedures. Finally, one two-dimensional and two three-dimensional test cases are presented to demonstrate the robustness and efficiency of the adjoint-optimized mesh deformation method.

## II. Mesh Deformation Strategy

The linear elasticity approach has been demonstrated by various authors[1,6,14] as a robust technique for computing dynamically deforming meshes. The motion of the computational mesh is assumed to obey the linear elasticity equations, which can be written as:

$$\frac{\partial \sigma_{ij}}{\partial x_i} = -f_j, \qquad \sigma = \mathbf{D}\epsilon, \qquad \epsilon = \mathbf{A}\delta\mathbf{x} \tag{1}$$

where, $\mathbf{D}$ is the constitutive matrix, which is a function of modulus of elasticity $E$. In three dimensions, the stresses $\sigma_{ij}$, strains $\epsilon_{ij}$, and displacements $\delta\mathbf{x}$ are given as:

$$\sigma = \{\sigma_{11}, \sigma_{22}, \sigma_{33}, \sigma_{12}, \sigma_{23}, \sigma_{31}\}^T, \qquad \epsilon = \{\epsilon_{11}, \epsilon_{22}, \epsilon_{33}, \epsilon_{12}, \epsilon_{23}, \epsilon_{31}\}^T, \quad \delta\mathbf{x} = \left\{ \begin{array}{ccc} \delta\mathbf{x}_1 & \delta\mathbf{x}_2 & \delta\mathbf{x}_3 \end{array} \right\}^T$$

By introducing the shape functions $M$, taken as linear functions over the mesh elements in our case, and applying a standard Galerkin method, we obtain

$$\mathbf{K}\delta\mathbf{x} = \mathbf{F} \tag{2}$$

where

$$\mathbf{K} = \int_\Omega \mathbf{B}^T \mathbf{D} \mathbf{B} dS, \quad \mathbf{F} = -\int_\Omega \mathbf{M}^T \mathbf{f} dS, \quad \mathbf{B} = \mathbf{A}\mathbf{M} \tag{3}$$

In the mesh deformation case, the boundary displacements are given, so that the external forces $f_j$, of the force vector $\mathbf{F}$ are not required. Rather, the homogeneous problem $\mathbf{K}\delta\mathbf{x} = 0$ is solved, subject to Dirichlet conditions on the $\delta\mathbf{x}$ displacement vector. Hence equation (2) can be rewritten as:

$$\mathbf{K}\delta\mathbf{x} = \mathbf{F}(\mathbf{x}_b) \tag{4}$$

where $\mathbf{x}_b$ is the boundary displacement vector and $\mathbf{F}(\mathbf{x}_b)$ is a function of $\mathbf{x}_b$. Note that the stiffness matrix $\mathbf{K} = \mathbf{K}(\mathbf{E})$ is a function of the E values in each cell, as seen from equation (3). One advantage of the linear elasticity approach, is that regions of large E (modulus of elasticity) will be displaced as a solid body. Thus, an appropriate prescription of the distribution of E can be used to avoid severe mesh deformation in critical regions of the mesh. In previous work, we have employed a distribution of E which is inversely proportional to the cell volume and/or to the distance from the deforming boundaries.[6,19] This turns out to be critical for avoiding invalid mesh cells in small cell regions and in regions near the boundaries.

While a distribution of the modulus E which is inversely proportional to the cell volume or to the distance from the deforming boundaries can minimize distortion for cells in critical near-body regions, negative volume cells may appear in unexpected regions of the domain for particular prescribed boundary displacements. An example is given in Figures 4a for the spoiler deflection problem discussed subsequently. Thus, a modulus distribution which not only prevents the cells near the body from becoming negative but also keeps other cells valid as the mesh deforms is crucial in order to take full advantage of the linear elasticity analogy. In the next section, we discuss the implementation of the adjoint approach for producing a more optimal distribution of E, and resulting in a more robust mesh deformation strategy.

## III. Adjoint-Based Optimization Procedure

In order to formulate the optimization problem for improving the robustness of linear-elasticity based mesh deformation methods, we must construct a suitable objective to be minimized, determine an efficient approach for computing the sensitivities of this gradient with respect to the design variables or model parameters, and make use of an efficient and practical optimization technique for obtaining an improved set of model parameters.

As opposed to shape optimization problems, where the design variables are used to define the shape of the geometry (usually two-dimensional), the set of design variables for the mesh optimization problem constitutes a three-dimensional set which involves the value of the modulus of elasticity in each mesh cell. Thus, the number of design variables will typically exceed several million, making the use of an adjoint-based approach imperative for gradient-based optimization methods. Additionally, a single objective function is desirable for the adjoint method, which accurately reflects the overall quality of the mesh and increases rapidly when negative volume cells are created. While the formulation of the adjoint problem is relatively straight-forward, the success of the mesh optimization problem in terms of robustness and efficiency depends critically on the choice of a suitable objective function, a good initial distribution of model parameters, and a robust optimization strategy.

### A. Objective Function

The mesh-deformation optimization problem is defined as minimizing an objective function $\mathbf{L}$ by varying the modulus of elasticity $E_i$ in each cell $i$, thus treating the $E_i$ as the design variables in an optimization framework. The objective function is designed in such a way that minimizing the objective function $\mathbf{L}$ will produce valid cells with minimal distortion in the deforming mesh. The objective function $\mathbf{L}$ is defined as a function of the cell volumes $\mathbf{V}$:

$$\mathbf{L} = \mathbf{L}(\mathbf{V}) \tag{5}$$

The construction of a suitable objective function for mesh-deformation optimization problems represents a non-trivial task. The objective should be representative of global mesh quality, and should increase rapidly for vanishing cell volumes. Additionally, the objective should be a convex function of the design variables in

order to facilitate the optimization procedure. For two-dimensional problems, the objective function given by

$$\mathbf{L} = \sum_{i=1}^{N} L_i \qquad \text{and} \qquad L_i = \begin{cases} \frac{a_-}{b_-^n}(\xi_i - 1)^n & \text{if } \xi_i \leq 0 \\ \frac{a_+}{b_+^n}(\xi_i - 1)^n & \text{if } \xi_i \geq 0 \end{cases} \tag{6}$$

has been found to be suitable for a wide range of problems, while the form given by

$$\mathbf{L} = \sum_{i=1}^{N} L_i \qquad \text{and} \qquad L_i = e^{a(\xi_i - 1)^n} - 1 \tag{7}$$

has been used for three-dimensional problems. In the above equations, $N$ is the total number of the design variables, $a_-$, $b_-$, $a_+$, $b_+$, $a$ and $n$ are the control coefficients and $n$ is set to an even positive number. The parameter $\xi_i$ in each cell is defined as $\xi_i = \frac{V_i}{V_{0i}}$, where $V_{0i}$ and $V_i$ are the volume of the $i^{th}$ cell before and after the deformation, respectively. Figure 1 provides an illustration of the objective functions described in equations (6) and (7). When $\xi_i$ equals unity, which corresponds to $V_i = V_{0i}$, $L_i$ vanishes. When $\xi_i$ approaches zero, which means the volume $V_i$ approaches zero, $L_i$ become very large. The objective function is designed in such a way that the cell volume $V_i$ is pushed towards the original cell volume $V_{0i}$ when the objective function is minimized by varying the design variables, thus avoiding collapsed cells as the mesh deforms. It should be noted that this optimization problem need not be completely convergent (i.e. the objective will not be reduced to zero) because cells usually cannot retain the same volume as the mesh is deformed.

### B. Adjoint Method

For a gradient based optimization strategy, we need to compute the sensitivity of the objective function with respect to all the design variables or model parameters, which in this case are the moduli of elasticity for each mesh cell. Because we will generally have millions of design variables, the adjoint method is used to compute these sensitivities. We consider the volume $V$ of a deformed mesh cell as a function of mesh point displacements $\delta\mathbf{x}$ and the initial coordinates of the mesh points $\mathbf{x}_0$:

$$\mathbf{V} = \mathbf{V}(\mathbf{x}_0 + \delta\mathbf{x}) \tag{8}$$

According to equation (4), the mesh deformations $\delta\mathbf{x}$ are a function of the prescribed boundary deformations $\mathbf{x}_b$, the coordinates of the initial mesh configuration $\mathbf{x}_0$ (which appears through the shape functions $M$), and the moduli of elasticity $E_i$, since different distributions of $\mathbf{E}$ will lead to a different stiffness matrix $\mathbf{K}(\mathbf{E})$ and thus different mesh displacements. Therefore, the mesh displacements can be written in the following functional form:

$$\delta\mathbf{x} = \delta\mathbf{x}(\mathbf{E}, \delta\mathbf{x}_b, \mathbf{x}_0) \tag{9}$$

which can be computed by solving the mesh motion equation

$$\mathbf{K}(\mathbf{E})\delta\mathbf{x} = \mathbf{F}(\delta\mathbf{x}_b) \tag{10}$$

The modulus coefficients $\mathbf{E}$ are the design variables and equation (5) can therefore be rewritten as

$$\mathbf{L} = \mathbf{L}(\mathbf{E}) \tag{11}$$

A variation in the design variables $\delta\mathbf{E}$ produces a corresponding variation of the objective $\delta\mathbf{L}$ as

$$\delta\mathbf{L} = \frac{d\mathbf{L}}{d\mathbf{E}}\delta\mathbf{E} \tag{12}$$

where the sensitivity derivative may be calculated (using equations (5) and (8)) as:

$$\frac{d\mathbf{L}}{dE_i} = \frac{d\mathbf{L}}{d\mathbf{V}}\frac{d\mathbf{V}}{d(\delta\mathbf{x})}\frac{\partial(\delta\mathbf{x})}{\partial E_i} \tag{13}$$

By differentiating equation (10) with respect to the $i^{th}$ design variable, we obtain

$$\frac{d\mathbf{K}}{dE_i}(\delta\mathbf{x}) + \mathbf{K}\frac{\partial(\delta\mathbf{x})}{\partial E_i} = 0 \qquad or \qquad \frac{\partial(\delta\mathbf{x})}{\partial E_i} = -\mathbf{K}^{-1}\frac{d\mathbf{K}}{dE_i}(\delta\mathbf{x}) \tag{14}$$

where $E_i$ is $i^{th}$ component of the vector $\mathbf{E}$ associated with cell $i$. Substituting equation (14) into equation (13), we get:

$$\frac{d\mathbf{L}}{dE_i} = \underbrace{-\frac{d\mathbf{L}}{d\mathbf{V}}\frac{d\mathbf{V}}{d(\delta\mathbf{x})}\mathbf{K}^{-1}}_{\Lambda^T}\frac{d\mathbf{K}}{dE_i}(\delta\mathbf{x}) \tag{15}$$

Defining $\mathbf{\Lambda}^T = -\frac{d\mathbf{L}}{d\mathbf{V}}\frac{d\mathbf{V}}{d(\delta\mathbf{x})}\mathbf{K}^{-1}$, we obtain the adjoint equation, which must be solved as:

$$\mathbf{K}^T\mathbf{\Lambda} = -\left(\frac{d\mathbf{L}}{d\mathbf{V}}\frac{d\mathbf{V}}{d(\delta\mathbf{x})}\right)^T \tag{16}$$

In equation (16), $\frac{d\mathbf{L}}{d\mathbf{V}}$ can be easily obtained by differentiating equation (6) or (7). Additionally, using the equality:

$$\frac{d\mathbf{V}}{d(\delta\mathbf{x})} = \frac{d\mathbf{V}}{d(\mathbf{x}_0 + \delta\mathbf{x})} = \frac{d\mathbf{V}}{d(\mathbf{x})} \tag{17}$$

the last term in equation (16) corresponds to the derivative of the deformed mesh cell volume with respect to the mesh coordinates, using the deformed mesh coordinates. This can easily be evaluated from the formulae used to compute the cell volumes. For example, the area of a two-dimensional triangle can be computed as:

$$V = \frac{1}{2}(c_1 b_3 - c_3 b_1) \tag{18}$$

where $b_1 = y_2 - y_3, \quad b_2 = y_3 - y_1, \quad b_3 = y_1 - y_2, \quad c_1 = x_3 - x_2, \quad c_2 = x_1 - x_3, \quad c_3 = x_2 - x_1$ using a cyclical indexing system $i = 1, 2, 3$ for the three vertices of the triangle. The required derivatives are then given as:

$$\frac{dV}{d(\delta\mathbf{x})} = \{b_1, c_1, b_2, c_2, b_3, c_3\}^T \tag{19}$$

For a three-dimensional tetrahedron, pyramid, prism or hexahedron, the volume may be computed as

$$V = \sum_{i=1}^{q} w_i \det\mathbf{J_i} \tag{20}$$

where, $w_i$ and $\mathbf{J_i}$ are the $i^{th}$ weight function and Jacobian matrix, respectively, and $q$ is the number of quadrature points. Then the required derivatives are given as:

$$\frac{dV}{d(\delta\mathbf{x})} = \sum_{i=1}^{q} w_i \frac{d(\det\mathbf{J_i})}{d\mathbf{x}} \tag{21}$$

Note that the $\frac{dV}{d(\delta\mathbf{x})}$ term is nominally a sparse matrix of size $ncells \times 3 \cdot npoints$, where $ncells$ represents the number of cells in the mesh, and $npoints$ denotes the number of mesh vertices, although only the locations corresponding to the vertices which constitute the corner points of a given element are non-zero. These terms can be assembled on the fly, and the resulting product $\frac{d\mathbf{L}}{dV}\frac{dV}{d(\delta\mathbf{x})}$ consists of a vector of length $3 \cdot npoints$, as required to make equation (16) dimensionally correct. Once the adjoint equation has been solved (c.f. equation (16)), the final sensitivity derivatives for all design variables can be obtained by performing the matrix vector multiplication:

$$\frac{d\mathbf{L}}{dE_i} = \mathbf{\Lambda}^T\frac{d\mathbf{K}}{dE_i}(\delta\mathbf{x}) \tag{22}$$

In practice, the calculation of the sensitivities, which must be performed at each design iteration, requires the solution of one mesh deformation problem (c.f. equation (10)), and one mesh adjoint problem (c.f. equation (16)). The solution of the mesh motion problem yields the values of the mesh point displacements

$\delta\mathbf{x}$, which are required both in equation (22) and for determining the right-hand side of the adjoint problem in equation (16). Next, the adjoint problem is solved, after which all terms are available for evaluating the right-hand-side of equation (22). The $\frac{d\mathbf{K}}{dE_i}$ term in this equation is easily obtained by differentiating the functional form of the stiffness matrix. Although this term represents a sparse matrix of dimension $3 \cdot npoints \times 3 \cdot npoints \times ncells$, only the terms corresponding to the corner points of a given cell are non-zero, and the matrix need not be evaluated explicitly. Rather, the complete sequence of matrix-vector products is assembled on an element basis, gathering the values from the corner points of each element, and scattering/accumulating the results back to these points. The final result consists of a vector of length $ncells$, as required to make the equation dimensionally consistent.
Rewriting equation (22) as:

$$\frac{d\mathbf{L}}{dE_i} = \mathbf{\Lambda}^T \frac{d\mathbf{K}}{dE_i}(\delta\mathbf{x}) = \mathbf{\Lambda}^T \frac{d\mathbf{K}}{dE_i}\mathbf{K}^{-1}\mathbf{F}(\delta\mathbf{x}_b) \tag{23}$$

clearly shows that the sensitivities required for the optimization problem depend on the particular prescribed boundary displacement $\delta\mathbf{x}_b$. Thus, different boundary displacements can be expected to result in different optimum E distributions. Furthermore, although we retain the linear form of the mesh motion equations, and the mesh adjoint equation is by definition a linear problem, the optimization problem itself (i.e. $\mathbf{L} = \mathbf{L}(\mathbf{E})$) is highly non-linear.

### C. Optimization Methods

The optimization procedure consists of finding the distribution of $\mathbf{E}$ which minimizes the objective function $\mathbf{L}$. At the $k^{th}$ iteration, the new distribution $\mathbf{E}_{k+1}$ is computed as:

$$\mathbf{E}_{k+1} = \mathbf{E}_k + \lambda_k \mathbf{p}_k \qquad \text{or} \qquad \Delta\mathbf{E}_k = \lambda_k \mathbf{p}_k \tag{24}$$

where $\lambda_k$ and $\mathbf{p}_k$ are the step length and the search direction, respectively. The steepest descent method represents a simple optimization algorithm[17] which has been used successfully for aerodynamic shape optimization.[5] In this approach, the search directions $\mathbf{p}_k$ are taken as $-\left(\frac{d\mathbf{L}}{d\mathbf{E}}\right)_k$. Once the objective function sensitivities $\left(\frac{d\mathbf{L}}{d\mathbf{E}}\right)_k$ have been computed using the method described above, an increment in the design variables is prescribed as:

$$\Delta\mathbf{E}_k = -\lambda\left(\frac{d\tilde{\mathbf{L}}}{d\mathbf{E}}\right)_k \tag{25}$$

where $\lambda$ is a small time step determined empirically, and $\left(\frac{d\tilde{\mathbf{L}}}{d\mathbf{E}}\right)_k$ is the smoothed gradient $\left(\frac{d\mathbf{L}}{d\mathbf{E}}\right)_k$. The advantage of the steepest descent method is its simplicity and suitability for optimization problems with large number of design variables. However the convergence speed of the steepest descent method was found to be very slow for the mesh optimization problems discussed in this paper. A better choice of the step length $\lambda$ or the search directions $\mathbf{p}_k$ can be used to help accelerate the convergence of the optimization problem. To this end, a line-search method[4,17] has been implemented to compute an appropriate step size $\lambda$ within the steepest descent approach. Defining a function

$$\phi(\lambda) = \mathbf{L}(\mathbf{E}_k + \lambda\mathbf{p}_k) \tag{26}$$

we attempt to find a step length $\lambda$ which minimizes the function $\phi$, or satisfies the Wofe condition (sufficient decrease condition):[17]

$$\mathbf{L}(\mathbf{E}_k + \lambda_k\mathbf{p}_k) \leq \mathbf{L}(\mathbf{E}_k) + c_1\lambda_k\left(\frac{d\mathbf{L}}{d\mathbf{E}}\right)_k^T \mathbf{p}_k \tag{27}$$

where $c_1$ is a constant and $0 < c_1 < 1$. Considering equation (26), the sufficient decrease condition (c.f. equation (27)) can be rewritten as

$$\phi(\lambda_k) \leq \phi(0) + c_1\lambda_k\phi'(0) \tag{28}$$

where $\phi'(0) = \left(\frac{d\mathbf{L}}{d\mathbf{E}}\right)_k^T \mathbf{p}_k$. If an initial guess $\lambda_0$ satisfies equation (28), then we set $\lambda_k = \lambda_0$. Otherwise, a quadratic function is constructed using the values of $\phi(0)$, $\phi'(0)$ and $\phi(\lambda_0)$:

$$\phi_q(\lambda) = a_q\lambda^2 + b_q\lambda + c_q \tag{29}$$

where the coefficients $a_q$, $b_q$ and $c_q$ are determined by $\phi_q(0) = \phi(0)$, $\phi'_q(0) = \phi'(0)$ and $\phi_q(\lambda_0) = \phi(\lambda_0)$. A new step length $\lambda_q$ can be found in $[0, \lambda_0]$ by minimizing the quadratic function (29):

$$\lambda_q = -\frac{\phi'(0)\lambda_0^2}{2(\phi(\lambda_0) - \phi(0) - \phi'(0)\lambda_0)} \tag{30}$$

If $\lambda_q$ satisfies equation (28), then let $\lambda_k = \lambda_q$. Otherwise, a cubic function is constructed using the values of $\phi(0)$, $\phi'(0)$, $\phi(\lambda_0)$ and $\phi(\lambda_q)$:

$$\phi_c(\lambda) = a_c\lambda^3 + b_c\lambda^2 + c_c\lambda + d_c \tag{31}$$

where the coefficients $a_c$, $b_c$, $c_c$ and $d_c$ are determined by $\phi_c(0) = \phi(0)$, $\phi'_c(0) = \phi'(0)$, $\phi_c(\lambda_0) = \phi(\lambda_0)$ and $\phi_c(\lambda_q) = \phi(\lambda_q)$. By minimizing equation (31), a new step length $\lambda_c$ in $[0, \lambda_q]$ is given by:

$$\lambda_c = \frac{-b_c + \sqrt{b_c^2 - 3a_c\phi'(0)}}{3a_c} \tag{32}$$

The algorithm described above is the so-called the cubic interpolation algorithm and is used in this paper to compute the step size $\lambda$. Additional details for the cubic interpolation algorithm can be found in references[4, 17]

Convergence of the optimization problem can also be improved using more sophisticated algorithms for computing improved search directions $\mathbf{p}_k$. In the BFGS algorithm,[4, 17] the search directions $\mathbf{p}_k$ in equation (24) are computed as:

$$\mathbf{p}_k = -\mathbf{B}_k \left(\frac{d\mathbf{L}}{d\mathbf{E}}\right)_k \tag{33}$$

where $\mathbf{B}_k$ is the inverse Hessian matrix and the size of $\mathbf{B}_k$ is $N \times N$, where $N$ is the number of design variables, which is typically of the order of several million. Storage of the $N \times N$ inverse Hessian matrix $\mathbf{B}_k$ is thus not practical for such large optimization problems. Therefore, we have also investigated the use of the limited memory BFGS method (LBFGS) presented by Liu and Nocedal,[7] since this approach does not require the storage of the Hessian matrix. Instead, an approximate inverse Hessian matrix $\mathbf{B}$ is computed at every iteration using $m$ vector pairs $\{s_i, y_i\}$:[7]

$$\begin{aligned} \mathbf{B}_k &= (\mathbf{Y}_{k-1}^T \cdots \mathbf{Y}_{k-m}^T)\mathbf{B}_k^0(\mathbf{Y}_{k-m} \cdots \mathbf{Y}_{k-1}) \\ &+ \rho_{k-m}(\mathbf{Y}_{k-1}^T \cdots \mathbf{Y}_{k-m+1}^T)\mathbf{s}_{k-m}\mathbf{s}_{k-m}^T(\mathbf{Y}_{k-m+1} \cdots \mathbf{Y}_{k-1}) \\ &\vdots \\ &+ \rho_{k-1}\mathbf{s}_{k-1}\mathbf{s}_{k-1}^T \end{aligned} \tag{34}$$

where $\mathbf{s}_k = \mathbf{E}_k - \mathbf{E}_{k-1}$, $\mathbf{y}_k = \left(\frac{d\mathbf{L}}{d\mathbf{E}}\right)_k - \left(\frac{d\mathbf{L}}{d\mathbf{E}}\right)_{k-1}$, $\rho_k = \frac{1}{\mathbf{y}_k^T\mathbf{s}_k}$ and $\mathbf{Y}_k = \mathbf{I} - \rho_k\mathbf{y}_k\mathbf{s}_k^T$. The initial Matrix $\mathbf{B}_k^0$ is a diagonal matrix and

$$\mathbf{B}_k^0 = \frac{\mathbf{y}_k^T\mathbf{s}_k}{\|\mathbf{y}_k\|^2}\mathbf{I} \tag{35}$$

By storing the $m$ previous values of the vectors $\{s_i, y_i\}$, the matrix $\mathbf{B}_k$ can be computed at each iteration implicitly. According to Liu and Nocedal,[7] $m$ is taken in the range $3 \sim 25$. In our computations, the value $m = 5$ is used. The search directions $\mathbf{p}_k = -\mathbf{B}_k \left(\frac{d\mathbf{L}}{d\mathbf{E}}\right)_k$ are then computed by a sequence of inner products $s_i$, $y_i$ and $\left(\frac{d\mathbf{L}}{d\mathbf{E}}\right)_k$. Further details on the LBGFS algorithm and the computation of $\mathbf{B}_k \left(\frac{d\mathbf{L}}{d\mathbf{E}}\right)_k$ are given by Noceal.[16]

## IV. Mesh Motion and Adjoint Solution Strategies

As mentioned previously, each design iteration involves the solution of one mesh motion problem (c.f. equation (10)) and one mesh adjoint problem (c.f. equation (22)). As with any optimization problem, two techniques are required to minimize the overall cost of the optimization. On the one hand, the use of sophisticated optimization algorithms such as the LBFGS method described above[17] are used to reduce the overall number of design cycles. On the other hand, the cost of each design cycle can be reduced by employing efficient solvers for the mesh motion and adjoint problems.

In previous work, we have demonstrated the use of agglomeration multigrid methods and line-implicit preconditioning, originally developed for accelerating the solution of the discretized flow equations,[9, 10] for

accelerating the solution of the mesh motion equations using either the spring analogy or the linear elasticity analogy.[19,20] In the current work, we use these techniques for efficiently solving the mesh motion equations, as well as the mesh adjoint equations.

The idea of a multigrid algorithm is to accelerate the solution on a fine grid by iteratively computing corrections to the fine grid problem on coarser grid levels where the cost of the iterations are lower, and the global error components are more easily reduced. For unstructured meshes, coarse multigrid levels can be constructed by grouping together or agglomerating fine level control volumes into a smaller set of coarser level control volumes, as shown in Figures 2a-b. Figure 2a shows the initial fine grid and the dual control volumes which are constructed around each mesh point, while Figure 2b shows the second level coarse grid where each coarse level control volume is a combination of several fine level control volumes.

For high-Reynolds number viscous flows, when highly stretched meshes are required to capture the thin boundary layer regions near the wall, the effectiveness of the multigrid approach degrades due to the anisotropic stiffness induced by the grid stretching. To relax this stiffness, an implicit line-solution technique was introduced in Reference.[10] The lines are constructed along the strong coupling direction in the mesh, as shown by the example depicted in Figure 2c for an unstructured mesh about a NACA0012 airfoil. In these regions, a block tridiagonal algorithm is used to solve all quantities along each line implicitly, thus replacing the simple explicit approach on all grid levels of the multigrid scheme.

A linear variant of the line-implicit agglomeration multigrid scheme is used to solve the mesh motion and adjoint problems, both of which are linear problems. While in theory, a duality preserving implementation of the multigrid algorithm can be used to guarantee similar convergence rates between the mesh motion and adjoint problems,[11,12,15] in practice the same multigrid solver is used on both problems, and similar convergence rates are generally observed for both problems, achieving suitable convergence in 50 to 100 multigrid cycles.

## V. Results and Discussion

Our first test case consists of a two-dimensional airfoil-spoiler configuration, which is a simplified model of a three-dimensional wing-body-spoiler configuration. The unstructured mesh is a viscous mesh with high stretching near the body, which includes approximately 8,700 vertices and 17,000 triangles, as shown in Figure 3. Figure 4a shows the deformed mesh generated by the linear elasticity analogy, with a modulus of elasticity prescribed as inversely proportional to the cell volume, as the spoiler rotates downwards 40 degrees. A region of invalid cells is clearly visible in the region between the spoiler and the airfoil, where the original cell sizes are not particularly small. The original modulus distribution (inversely proportional to the cell volume or the distance from the wall) is inadequate for preventing the volume of these cells from becoming negative. The objective function used in this case is that given by equation (6). The coefficients are set as: $a_- = a_+ = 0.1$, $b_- = b_+ = 0.5$, and $n = 4$. The optimization procedure acts by identifying the influence of these areas on the global objective, and increasing the critical local modulus (E) variables accordingly. Figure 4b shows the mesh generated using the optimal distribution of the modulus E, as determined by the optimization procedure, illustrating the elimination of all negative volume cells. Figures 5a and 5b depict the initial and final modulus E distributions, demonstrating how the optimization process results in increased E values in the region of collapsing mesh cells between the spoiler and the airfoil, thus eliminating the invalid cells produced with the original prescribed E distribution.

Figure 6a shows the convergence of the line-implicit multigrid algorithm for the mesh motion equations and the mesh adjoint equations, respectively. Both problems converge at similar rates, and the residuals are reduced by approximately 8 to 10 orders of magnitude in 100 multigrid cycles for both problems in this case. Figure 6b compares the performance of the various optimization algorithms in recovering a valid grid, by plotting the minimum cell volume versus the number of design cycles. The LBFGS method produces a valid grid (recovering all negative cells) in 6 design iterations, whereas the steepest descent method with the line-search algorithm has not completely eliminated all negative cells after 18 iterations. The steepest descent method with constant $\lambda$ produces an almost flat cure, indicating that this approach is impractical, since a very large number of design iterations are needed to eliminate all invalid cells. In these plots, a design iteration is defined as a mesh motion and adjoint solution because the time spent in the optimization algorithm is trivial compared to the time required for the mesh motion and adjoint solutions.

The second test case consists of a three-dimensional landing-gear configuration, which includes approximately 600,000 grid points and 1.4 million cells. The unstructured grid consists of a viscous hybrid mesh,

which contains mixtures of tetrahedra, pyramids and prisms. Figure 7a shows the surface mesh of the landing-gear configuration. A twisting motion, as depicted in Figure 7b, is prescribed on the geometry in order to test the mesh deformation procedure. For a twisting angle of 12 degrees, the deformed mesh computed by the linear elasticity approach with a modulus of elasticity E prescribed as inversely proportional to the cell volume, results in 121 negative volume cells in the region between the two converging wheel geometry boundaries, as depicted in Figure 7c.

For the optimization problem, the objective function used in this case is given by equation (7). The coefficients are set as: $a = 5$ and $n = 2$. Figure 8a shows the convergence of the multigrid algorithm for the mesh motion equations and the mesh adjoint equations, where the residuals for both problems are reduced by five orders of magnitude in approximately 50 line-implicit multigrid cycles. In Figure 8b the LBFGS optimization algorithm is seen to result in a valid mesh in 10 design iterations, while the steepest descent method with the line-search algorithm eliminates all negative cells in 20 iterations. The steepest descent method with constant step size $\lambda$ fails to produce a valid mesh after 30 iterations.

The final test case is a more complicated three-dimensional wing-body-flap-engine configuration, which consists of a fuselage, main wing, leading-edge slat, double slotted trailing-edge flaps, and a nacelle-pylon configuration, as shown in Figure 9. The unstructured mesh is a highly stretched viscous hybrid mesh which consists of approximately 3 million grid points and a total of 11 million cells (tetrahedra, pyramids and prisms). There are many small gaps between the leading/trailing-edge flaps and the main wing, as shown in Figure 9. A twisting motion is prescribed on the main wing-flap assembly, while the trailing-edge flap is also prescribed a 10 degree pitching motion, as shown in Figure 10. The deformed mesh generated by the linear elasticity approach with the modulus E prescribed as inversely proportional to the cell volume results in a total of 46 negative volume cells in the flap gap region, as shown in Figure 11.

The objective function used for the optimization problem in this case is given by equation (7). The coefficients are set as: $a = 1$ and $n = 2$. Figure 12a depicts the convergence of the line-implicit multigrid algorithm for the mesh motion equations and the mesh adjoint equations, where the residuals of the mesh motion equations are reduced by 6 orders of magnitude over 150 multigrid cycles, while the residual for the mesh adjoint equations are reduced by approximately 2.5 orders of magnitude over 150 multigrid cycles. The slower convergence of the adjoint problem for this case is unexpected, although the overall impact on the optimization problem was found to be minimal. In Figure 12b the LBFGS algorithm recovers a valid grid in 6 design iterations, while the steepest descent approach with the line-search algorithm fails to recover a valid mesh after 15 design cycles.

In the above examples, one design cycle or optimization iteration represents a single mesh motion and mesh adjoint solution. For the line-search and LBFGS algorithms, these function calls may be used either to update the E distribution, or to improve the step size and search direction estimates. For each design iteration, the time spent in the optimization algorithm is trivial compared to the time required for the mesh motion and adjoint solutions. The cost of a mesh adjoint solution is equivalent to the cost of a mesh motion solution, since both problems contain the same number of unknowns and converge at similar rates. From the above test cases, the LBFGS algorithm is seen to require of the order of 5 to 10 design cycles to produce a valid grid. Thus, the mesh optimization problem requires roughly one order of magnitude additional cpu time over a single linear elasticity mesh deformation calculation. In previous work,[20] we have compared the cost of solving the mesh deformation problem with the cost of solving an implicit time step for the flow equations, using the line-implicit agglomeration multigrid algorithm for both problems. The mesh motion problem was found to require between 20% and 35% of the cpu time required for the solution of the flow equations at an implicit time step. Therefore, invoking the mesh optimization procedure at each implicit time step within an unsteady flow calculation will not be practical. Rather, the mesh optimization procedure can be employed as a plug-in module which is called at critical time steps in the simulation in order to repair the mesh when negative volume or poor quality cells are detected. Alternatively, if the geometry motion is prescribed, an optimal E distribution can be precomputed for the most severe deformation case and employed throughout the simulation with the linear elasticity mesh deformation equations. For aeroelasticity problems, where the geometry motion is computed as part of the solution, optimal E distributions may be computed for each modal displacement, and linear combinations of these distributions may be formed during run time, based on the modal response of the structure, or a multi-point optimization problem may be formulated.

## VI. Conclusion

An optimization procedure for linear-elasticity-based mesh deformation techniques has been formulated and validated in this work. The technique seeks to compute an optimal distribution of the modulus of elasticity used in the linear-elasticity analogy, in order to enhance the robustness and extend the range of applicability of this mesh deformation techniques for large displacement cases.

Note that an alternate optimization approach would be to simply use the grid point coordinates as the design variables in order to minimize the mesh deformation objective function, as proposed in reference.[8] However, our approach of using a linear elasticity analogy and optimizing the distribution of E within this framework is designed, on the one hand, to capitalize on the solid-body displacement preservation property of the linear elasticity method for regions with high E. On the other hand, we are also able to start with a good initial guess for the distribution of E (i.e. inversely proportional to the cell size, or distance from the wall), which should make the optimization problem much more local and thus tractable, as compared to a brute force approach based on grid point coordinates.

While our proposed optimization procedure is successful at removing distorted or negative volume cells for difficult mesh deformation problems, the optimal E distributions depend on the imposed boundary displacements, and the optimization procedure generally requires an order of magnitude more computational effort than a simple linear-elasticity mesh deformation calculation. The optimization procedure is thus best suited for use as a plug-in module which is invoked when the non-optimized mesh deformation approach fails, or for precomputing optimal modulus of elasticity distributions which can be used in subsequent simulations.

Future work will concentrate on improving the efficiency of the solution of the optimization problem, including the use of more powerful optimizers, experimentation with different objective functions, and the effect of partially converging intermediate mesh motion and adjoint problems at intermediate design iterations. The formulation of multi-point optimization problems for pre-computing optimal E distributions for a range of possible mesh motion problems will also be investigated.

## VII. Acknowledgments

The first author would like to thank Dr. M. Nemec, NASA Ames Research Center, for help on the optimization methods. This work was supported in part by grant NNL04AA63G from the NASA Langley Research Center.

## References

[1]T. Baker and P. A. Cavallo. Dynamic adaptation for deforming tetrahedral meshes. AIAA Paper 1999-3253, 1999.

[2]J. T. Batina. Unsteady Euler airfoil solutions using unstructured dynamic meshes. *AIAA Journal*, 28(8):1381–1288, 1990.

[3]C. Farhat, C. Degand, B. Koobus, and M. Lesoinne. Torsional spring for two-dimensional dynamic unstructured fluid meshes. *Computer Methods in Applied Mechanics and Engineering*, 163:231–245, 1998.

[4]J. J. E. Dennis and R. B. Schnabel. *Numerical Methods For Unconstrained Optimization And Nonlinear Equations*. Prentice-Hall, Inc., 1983.

[5]A. Jameson, J. J. Alonso, J. J. Reuther, L. Martinelli, and J. C. Vassberg. Aerodynamic shape optimization techniques based on control theory. AIAA Paper 1998-2538, 1998.

[6]A. A. Johnson and T. E. Tezduyar. Simulation of multiple spheres falling in a liquid-filled tube. *Computer Methods in Applied Mechanics and Engineering*, 134:351–373, 1996.

[7]D. C. Liu and J. Nocedal. On the limited memory BFGS method for large scale optimization. *Mathematical Programming*, 45:503–528, 1989.

[8]E. J. Lopez, N. M. Nigro, M. A. Storti, and J. A. Toth. A minimal element distortion strategy for computational mesh dynamics. *International Journal for Numerical Methods in Engineering*, 2006.

[9]D. J. Mavriplis. Multigrid techniques for unstructured meshes. In *VKI Lecture Series*, number 1995-02 in VKI-LS. 1995.

[10]D. J. Mavriplis. Multigrid strategies for viscous flow solvers on anisotropic unstructured meshes. *Journal of Computational Physics*, 145(1):141–165, Sept. 1998.

[11]D. J. Mavriplis. A discrete adjoint-based approach for optimization problems on three-dimensional unstructured meshes. AIAA Paper 2006-0050, (to appear in AIAA Journal), Jan. 2006.

[12]D. J. Mavriplis. Multigrid solution of the discrete adjoint for optimization problems on unstructured grids. *AIAA Journal*, 44(1):42–50, Jan. 2006.

[13]M. Murayama, K. Nakahashi, and K. Matsushima. Unstructured dynamic mesh for large movement and deformation. AIAA Paper 2002-0122, 2002.

[14]E. J. Nielsen and W. K. Anderson. Recent improvements in aerodynamic optimization on unstructured meshes. *AIAA Journal*, 40(6):1155–1163, June 2002.

[15]E. J. Nielsen, J. Lu, M. A. Park, and D. L. Darmofal. An implicit exact dual adjoint solution method for turbulent flows on unstructured grids. *Computers and Fluids*, 33(9):1131–1155, Nov. 2004.

[16]J. Nocedal. Updating Quasi-Newton matrices with limited storage. *Mathematics of Computation*, 35(151):773–782, July 1980.

[17]J. Nocedal and S. Wright. *Numerical Optimization*. Springer, 2000.

[18]V. Venkatakrishnan and D. J. Mavriplis. Implicit method for the computation of unsteady flows on unstructured grids. *Journal of Computational Physics*, 127:380–397, 1996.

[19]Z. Yang and D. J. Mavriplis. Unstructured dynamic meshes with higher-order time integration schemes for the unsteady Navier-Stokes equations. AIAA Paper 2005-1222, 2005.

[20]Z. Yang and D. J. Mavriplis. Higher-order time integration schemes for aeroelastic applications on unstructured meshes. AIAA Paper 2006-441, (to appear in AIAA Journal), 2006.

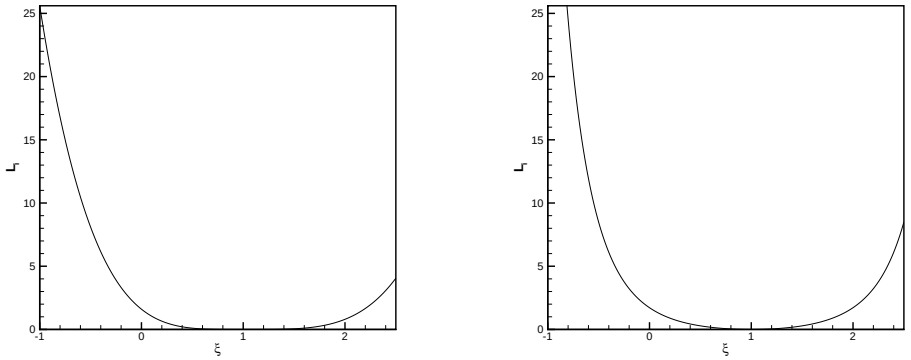


(a) (b)

**Figure 1. (a) Illustration of the variation of the global objective function defined in equation (6) with respect to the volume ratio $\xi$ at a single cell using the parameter values $a_- = a_+ = 0.1$, $b_- = b_+ = 0.5$, $n = 4$. (b) Illustration of the variation of the global objective function defined in equation (7) with respect to the volume ratio $\xi$ at a single cell using the parameter values $a = 5$ and $n = 2$.**

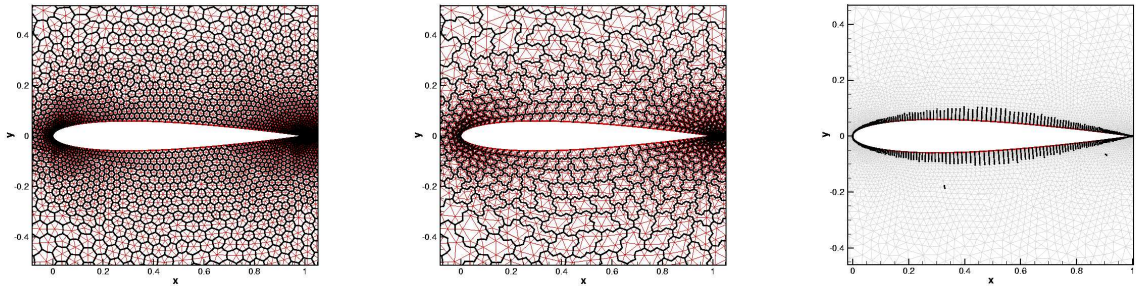


(a) 1st level (b) 2nd level (c) implicit lines

**Figure 2. Illustration of (a) fine mesh and dual control volume structure used for coarse level agglomeration multigrid construction, (b) first coarse level agglomerated grid, and (c) line structures used in boundary layer regions for implicit line solver.**

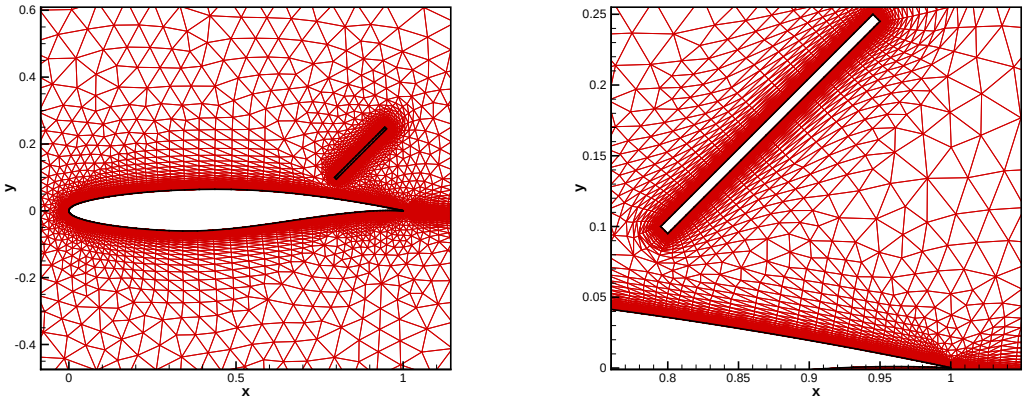


(a) (b)

**Figure 3. Illustration of initial two-dimensional unstructured mesh for spoiler deflection problem with high stretching in boundary layer regions.**

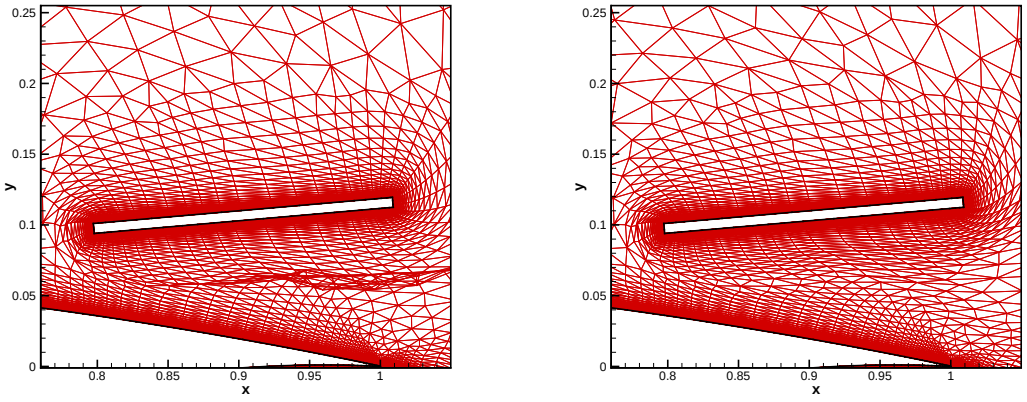


(a) (b)

**Figure 4. (a) Deformed mesh for spoiler deflection problem using prescribed E distribution illustrating region of invalid mesh cells, (b) Deformed mesh for spoiler deflection problem using optimized E distribution illustrating recovery of valid mesh cells throughout the domain.**

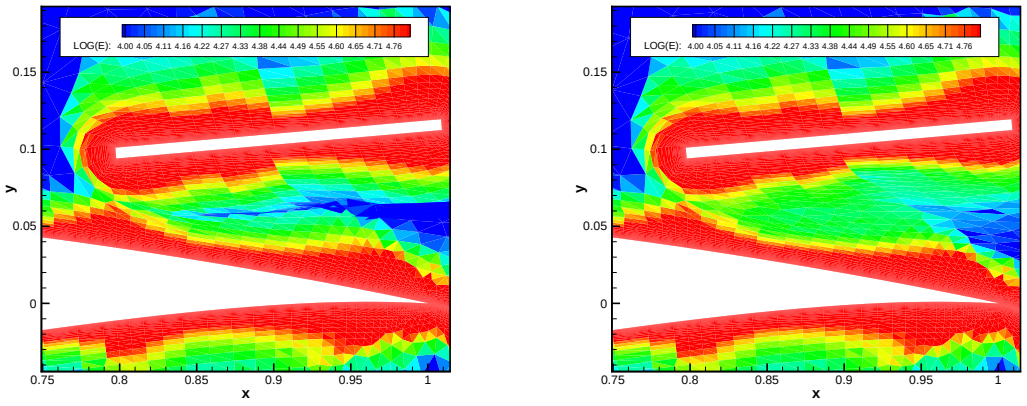


(a) (b)

**Figure 5. (a) Prescribed modulus E distribution in deformed spoiler mesh, and (b) Optimized modulus E distribution in deformed spoiler mesh.**

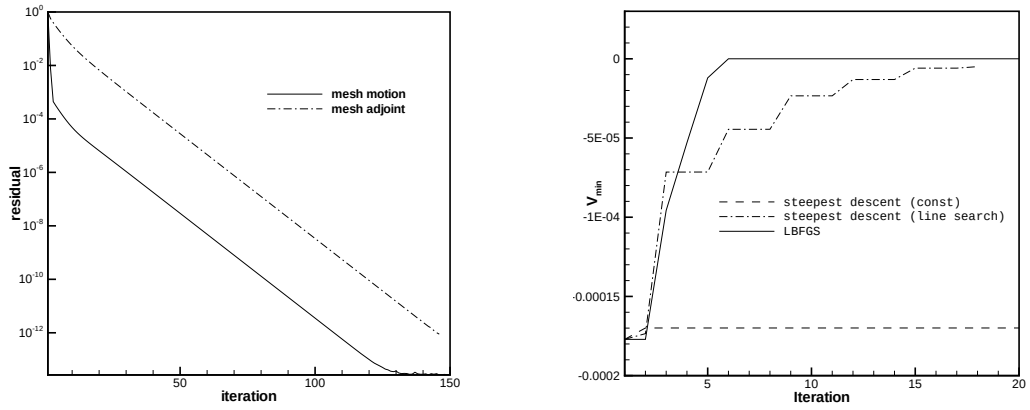


(a) (b)

**Figure 6. (a) Convergence history of line-implicit multigrid solver for mesh deformation and mesh adjoint equations for two-dimensional spoiler deflection case and (b) Convergence of the various optimization strategies for two-dimensional spoiler deflection case as measured by the number of optimization cycles requires to recover mesh with fully positive volume cells.**

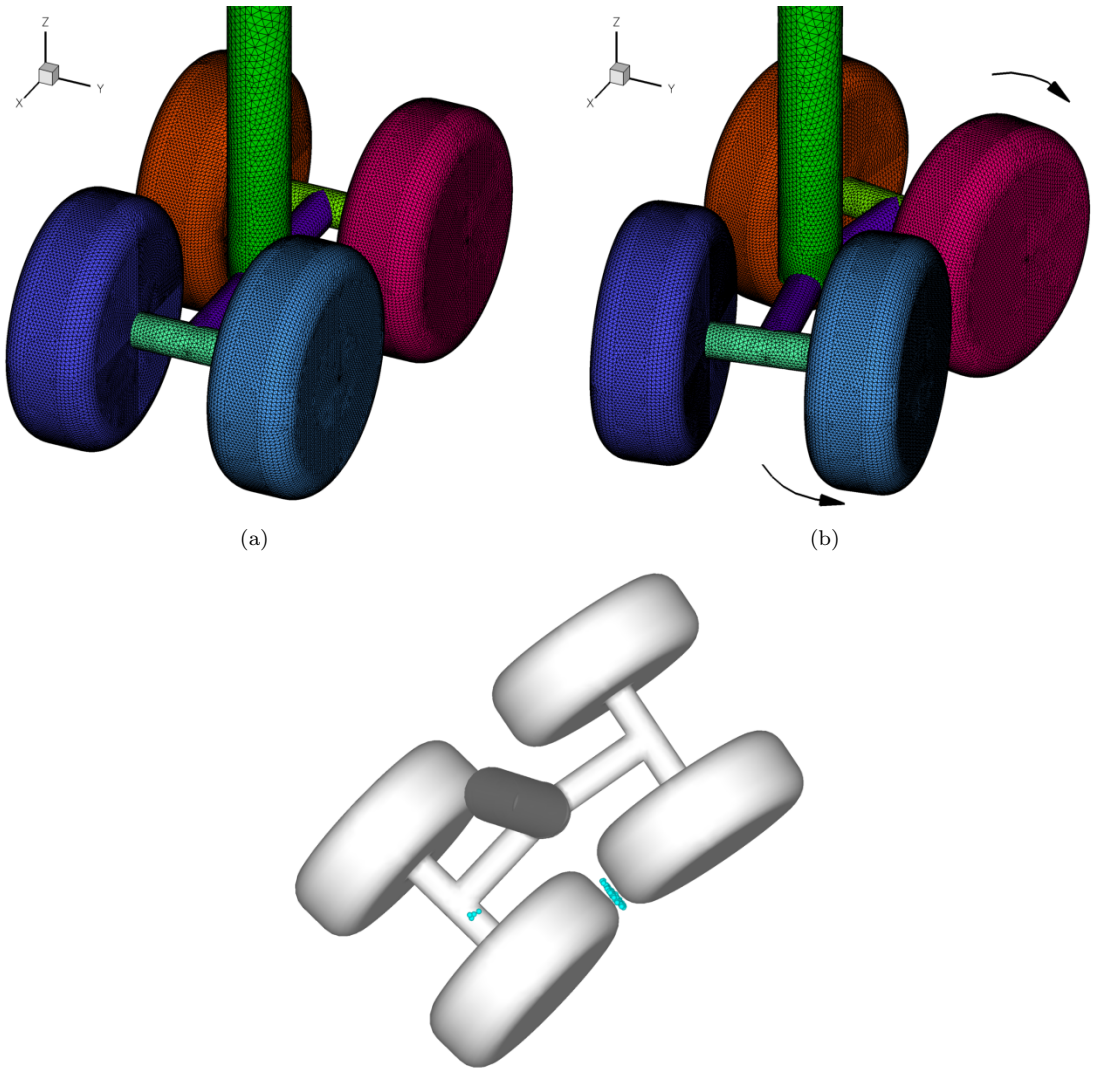


(a) (b)

(c)

**Figure 7. Illustration of (a) initial and (b) deformed mixed element mesh (containing tetrahedral, prismatic and pyramidal cells) on landing gear configuration and (c) location of negative cells for deformed mesh using original prescribed modulus E distribution. Number of points = 600,000. Number of cells = 1.4 million.**

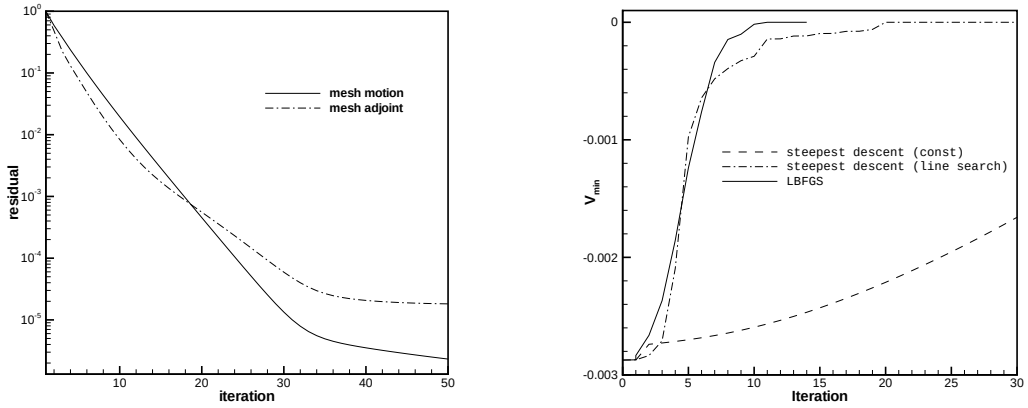


(a) (b)

**Figure 8. (a) Convergence history of line-implicit multigrid solver for mesh deformation and mesh adjoint equations for three-dimensional landing-gear case and (b) Convergence of the various optimization strategies as measured by the number of optimization cycles requires to recover mesh with fully positive volume cells.**

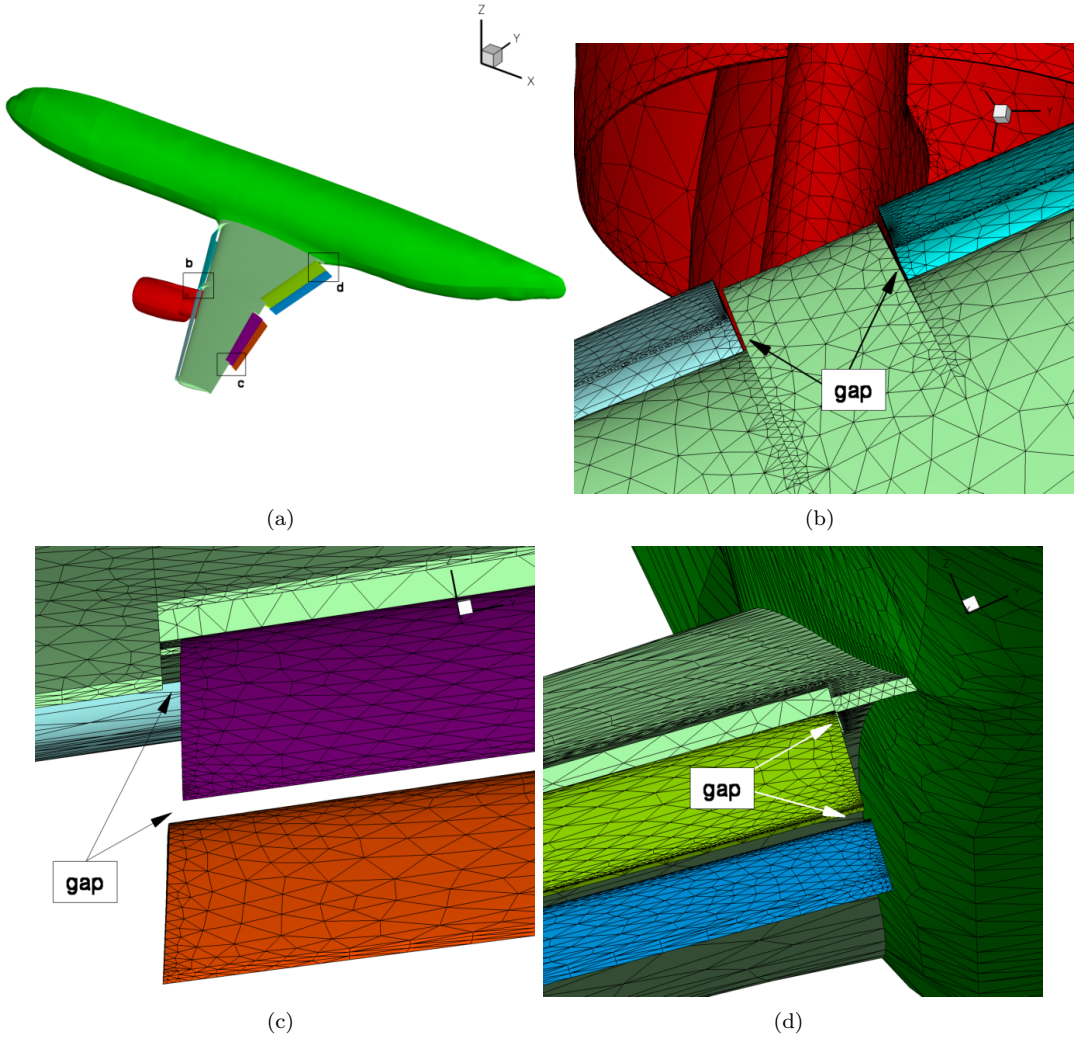


(a) (b)

(c) (d)

**Figure 9. Illustration of surface mesh on complex wing-body-slat-flap-nacelle-pylon geometry and location of critical gap regions. Hybrid mesh contains 3 million points and 11 million cells (tetrahedra, prisms, pyramids).**

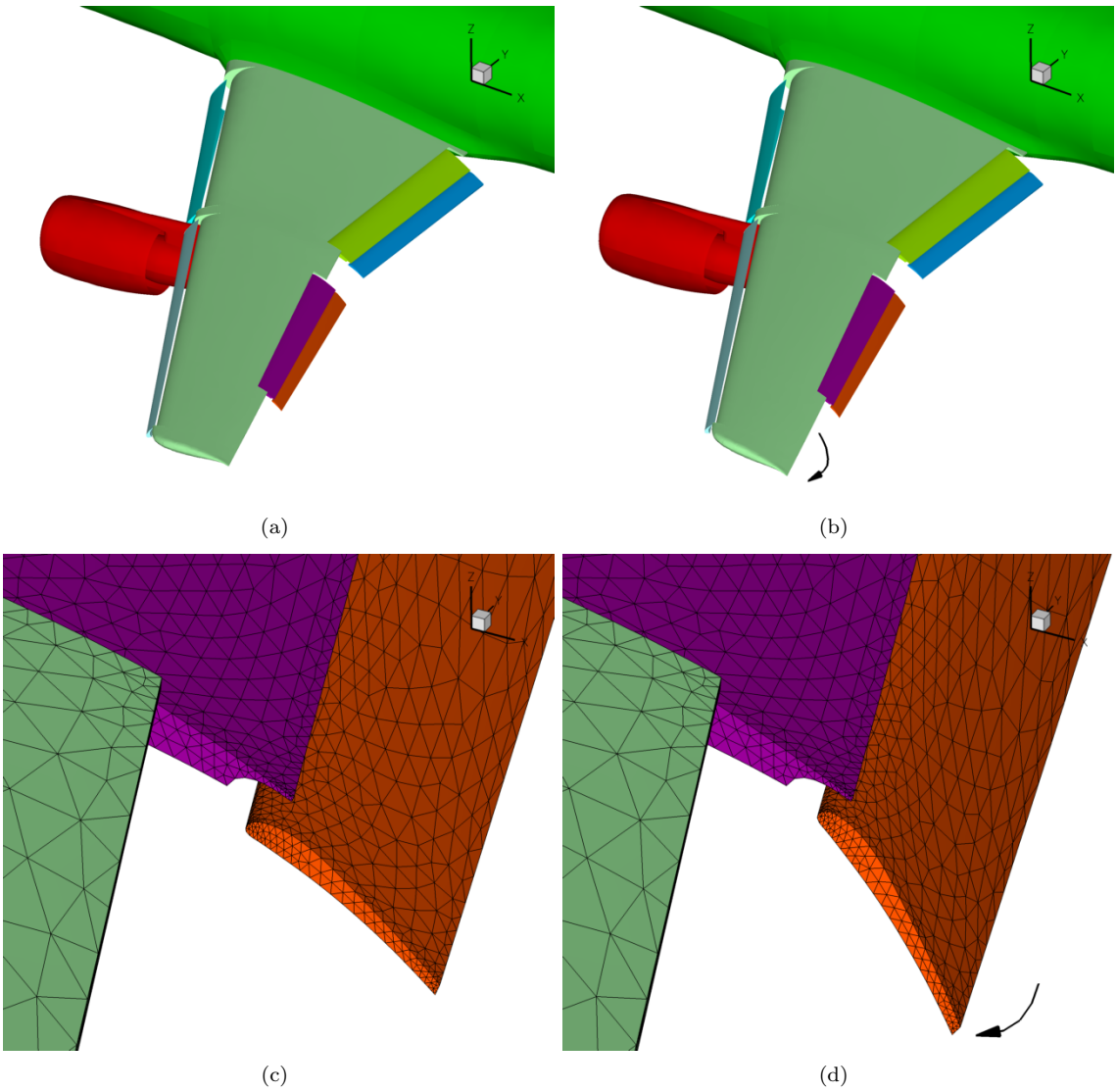

**Figure 10. Illustration of (a-b) wing twisting and (c-d) flap pitching motion imposed on geometry for mesh deformation test case.**

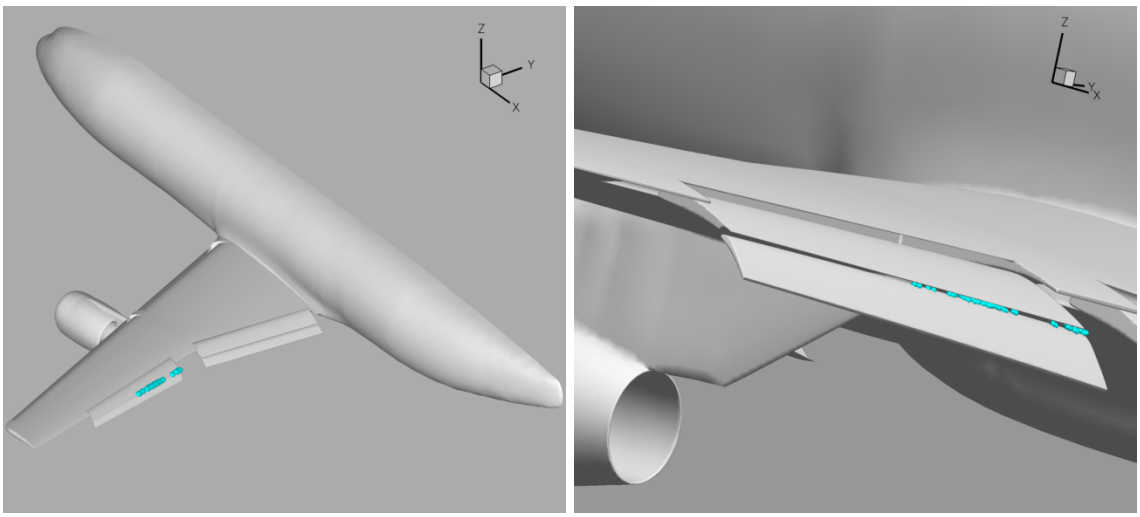


(a) (b)

**Figure 11. Location of negative cells produced by mesh deformation solution using prescribed modulus E distribution.**

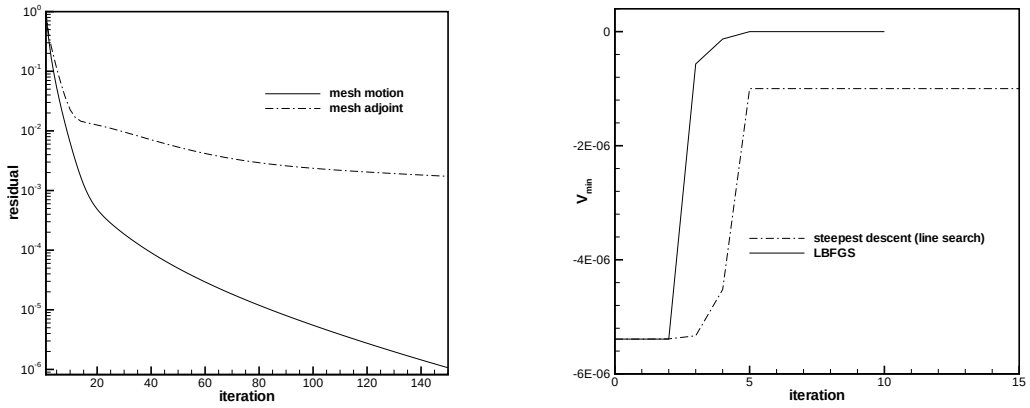


(a) (b)

**Figure 12. (a) Convergence history of line-implicit multigrid solver for mesh deformation and mesh adjoint equations for three-dimensional complex wing-body-slat-flap-nacelle-pylon geometry (b) Convergence of the various optimization strategies as measured by the number of optimization cycles requires to recover mesh with fully positive volume cells.**